# PEDESTRIAN-VEHICLE INTERACTION: KINEMATICS AND INJURY ANALYSIS OF FOUR FULL-SCALE TESTS

**Damien Subit, Jason Kerrigan, Jeff Crandall**
**Center for Applied Biomechanics, University of Virginia, Charlottesville, USA**

**Keisuke Fukuyama, Kunio Yamazaki**
**Japan Automotive Research Institute, Tsukuba, Japan**

**Koichi Kamiji, Tsuyoshi Yasuki**
**Japan Automobile Manufacturers Association, Tokyo, Japan**

## ABSTRACT

The goal of this study was to describe the kinematics and injuries of a pedestrian hit by a vehicle. Four full scale cadaver tests were performed with a small city car and a mid-sized sedan traveling at 40 km/h. For each vehicle type, a short and a small subject was set in a well defined initial position in order to compare response differences related to anthropometric variation. For each body region sustaining trauma, injury mechanisms were determined based on the pedestrian kinematics and the deformation of the vehicle. The kinematics of the pelvis were shown to depend on the subject stature relative to the vehicle geometry and were found to be a primary factor in determining whole body kinematics and injury patterns.

**Keywords:** cadaver, crashworthiness, kinematics, pedestrians, sled tests

**PEDESTRIAN CRASHES** are the most frequent cause of traffic-related fatalities worldwide with the World Bank (2003) estimating that between 41% and 75% of all road traffic fatalities are pedestrians. New regulations for pedestrian protection as well as increased socio-political interest in making roads safer for all road-users requires an understanding of how injuries to pedestrians can be reduced by improving vehicle design. Due to the great complexity of the pedestrian-vehicle impact, the numerous types of vehicles in the fleet, and the large range in pedestrian stances (Meissner *et al.*, 2004), describing the pedestrian-vehicle interaction requires performing numerous tests to understand the range of possible pedestrian kinematics and injury mechanisms. One effective way to assess pedestrian kinematics and injuries is to perform full scale cadaver tests. The goal of the present study was to describe the vehicle-pedestrian impact interaction by linking the injuries sustained by the pedestrian to its anthropometry and the design and deformation of the front-end structures of the vehicles. To achieve this goal, four full-scale cadaver tests were performed with a mid-sized sedan and a small city car. A particular effort was undertaken to determine the deformation of the vehicle front-end structures since it has been shown that the vehicle geometry and stiffness have a large affect on both pedestrian kinematics and injuries (Bunkertorp et al, 1983; Kallieris and Schmidt, 1988). By combining kinematic data, vehicle deformation information, and injuries sustained, the paper identifies potential injury mechanisms and their dependence on anthropometry of the subjects relative to the vehicle geometry.

## MATERIALS AND METHODS

Cadaver tests were performed with a mid-sized sedan (MSS) and a small city car (SCC) using a custom deceleration sled. To examine the potential influence of anthropometry on pedestrian response each vehicle was tested with a short and a tall subject. Details of the sled system, buck preparation, subject preparation, and the associated instrumentation are described in the following sections.

TEST OVERVIEW : While the test system used to perform these tests has been previously described by Kam *et al.* (2005), Kerrigan *et al.* (2005, 2007) and Untaroiu *et al.* (2007), the main features are briefly described here. The test system consists of a sled track onto which a vehicle buck is accelerated to 40 km/h before impacting the pedestrian. The vehicles were production versions of a small city car and a mid-sized sedan which were cut rearward of the B-pillar and attached to the sled (Fig. 1). In an effort to reduce variability and simplify the system, the wheels, the suspension, and the engine were removed. The pedestrian was positioned on a second smaller sled (Fig. 5), designed to mimic the height of the ground

level with respect to the vehicle. Once the vehicle passed a trigger attached to the sled, the subject was released in order to allow for an unconstrained interaction with the vehicle. The subjects were fully released at least 11 ms before the pedestrian/vehicle contact was initiated. The vehicle buck struck pedestrian sled (Fig. 5) and both were stopped by a hydraulic decelerator system. A catching system was installed at the end of the track to catch the pedestrian in order to prevent injuries from secondary contact with the ground. The vehicle bucks were inspected after each test and the damaged parts were replaced.

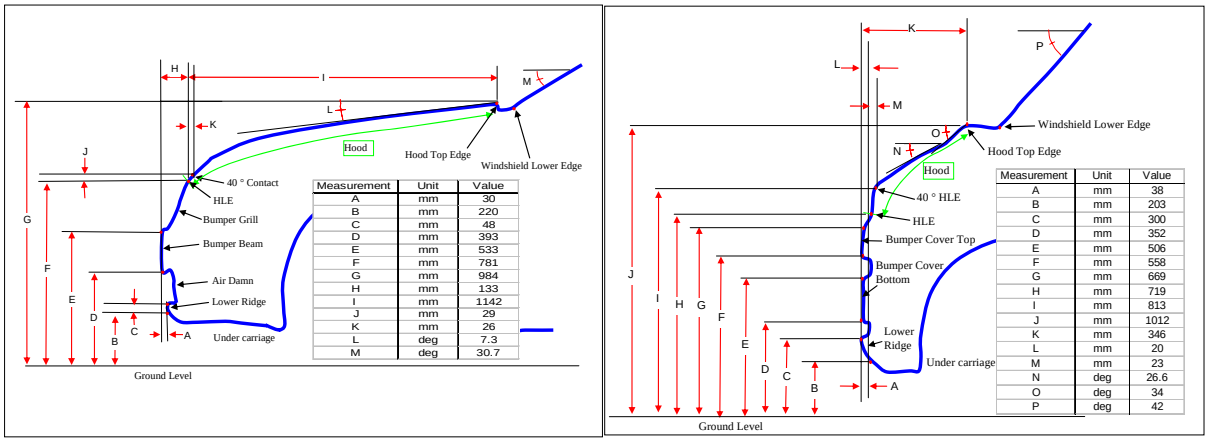


**Fig. 1 - Schematic of the centerline cross-section of the mid-sized sedan (*left*) and small city car (*right*). The 40° HLE (Hood Leading Edge) position is the EEVC reference line (EEVC, 1998).**

VEHICLE PREPARATION : The vehicle body parts were painted with a flat chalk-based paint to minimize the reflection of the light required for high-speed video. The vehicle center line was marked with tape from the bottom of the bumper to the top of the windshield. From the center line, a parallel line was marked every 100 mm from the left to the right side of the vehicle. In a similar fashion, the vehicle wrap around distances (WAD) were marked every 100 mm from 800 mm to the top of the windshield (2200 mm for MSS, 1900 mm for SCC). Extra lines were added every 50 mm in both directions in the area where the pedestrian was likely to contact. The hood leading edge reference line as defined by the EEVC (1998) and the 1250 mm WAD were also marked. Finally, a grid of roughly 500 phototargets was created from the intersections of the vertical and horizontal lines. The locations of these phototargets was measured before and after each test with a 3D coordinate measurement machine (CMM, Titanium Faro arm) to evaluate the vehicle deformation.

SUBJECT PREPARATION

Subjects anthropometry: Four male cadavers were selected for this study based on the absence of pre-existing fractures and lesions or other bone pathology (Table 1.). The cadavers were obtained and treated in accordance with established ethical guidelines and all testing and handling procedures were reviewed and approved by an independent oversight committee at the University of Virginia. Bone mineral densities were measured from standard femoral neck/trochanteric readings obtained by Dual Energy X-ray Absorptometry (DEXA) readings. The T-score represents the number of standard deviations above/below the mean for a young adult of the same gender at peak bone mineral density while the Z-score is the number of standard deviations above/below the mean for adults of the same age, race and gender.

**Table 1 - Subject information.**

| Test | Age (year) | stature(cm) / Mass (kg) | Cause of death | Bone mineral density (g/cm$^2$) | T-score | Z-score | WHO classification |
|---|---|---|---|---|---|---|---|
| MSS-S | 62 | 154 / 72.6 | Coronary artery disease | 0.753 | - 1.9 | - 1.4 | Osteopenia |
| MSS-T | 62 | 183 / 114 | Skin cancer | 0.975 | - 0.4 | 0.1 | Normal |
| SCC-S | 64 | 161 / 86.2 | Chronic obstructive pulmonary disease | 0.776 | - 1.7 | - 1.2 | Osteopenia |
| SCC-T | 67 | 182 / 46.3 | Lung cancer | 0.638 | - 2.6 | - 2 | Osteoporosis |

Instrumentation: Each specimen was instrumented with seven six-degree-of-freedom packages (6DOFP) consisting of three angular rate sensors (ATA ARS-06 magnetohydronamical sensors) and three linear accelerometers (Endevco 7264-2000), arranged in a cube housing to allow measurement of both accelerations in and angular velocities about the three orthogonal axes 1, 2 and 3 (Fig. 2). The package

measures 44×44×31 mm and weighs 180 g. The three points circled in Fig. 2 are reference points used to determine the position and the orientation of the sensor packages from the CMM data obtained prior to the impact (see subsection Initial position).

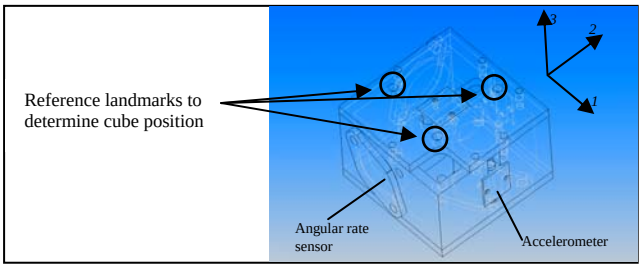


**Fig. 2 - Schematic of a 6DOFP.**

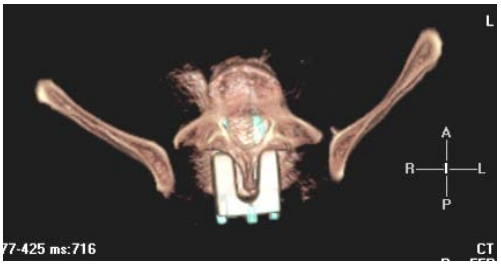


**Fig. 3 – Superior view of the L5 U-mount.**

These sensor packages were affixed to the head, T1 vertebra, L5 vertebra, right and left femora, right and left tibiae, through specific hardware mounts which allowed for a rigid attachment of the 6DOFP to the bony parts. The L5 vertebra was designated as a convenient whole body reference so particular emphasis was placed on the instrumentation at this location. An aluminum U mount (Fig. 3) specifically designed to accommodate the shape of this vertebra was affixed to the posterior aspect with two deep-threaded screws that passed through the lamina and terminated in the vertebral body. The 6DOFP was attached to the posterior side of the U mount (Fig. 3). A full-body CT-scan (slice thickness: 0.625mm, planar resolution: 0.98 mm/pixel) was performed to locate the position of the mounts with respect to the body segment to which they were attached (see Data processing section). An on-board data acquisition system (DTS TDAS G5, front-end hardware filter cut-off frequency: 4 kHz) affixed to the subjects sampled the data from -40 to 250 ms at 10 kHz (0 is the time of first contact between the subject's right leg and the vehicle).

HIGH SPEED VIDEOS : Phototargets were affixed to each subject at anatomical landmarks, as well as on top of each 6DOFP (Fig. 4 left). Two targets were affixed to the left fender of the vehicle. Five cameras (2 posterior views, 1 anterior view, 1 oblique views) recorded the motion at 1000 fps from - 20ms to 250 ms, which was after the time of contact of the head with the vehicle. The targets were tracked on the videos from -20 ms to a few milliseconds after the contact of the head with the windshield.

FINAL PRE-TEST PREPARATIONS: After completing the instrumentation and target installation, the subject was dressed in tight-fitting cotton thermal underwear to ensure a realistic interaction between the subject and the vehicle. The bare feet of the subject were positioned on foam insulation (25 mm thick) to simulate the increase in subject height due to shoes. The subject was positioned laterally with respect to the vehicle, in mid-stance gait, with the right (struck-side) leg back, and was held in position by two harnesses made of pieces of seatbelt webbing (Fig. 4 right). The position of the harnesses was adjusted such that almost all the subject's weight was supported by the shoulder harness, whereas the head harness was used to maintain the head in an upright and neutral position. Both harnesses were attached to the release mechanism. Measurements were taken during positioning (distances between the feet, and orientation of the thighs and the legs) to ensure the reproducibility of the position between tests. The on-board data-acquisition system (TDAS) was securely affixed to the back of the subject and triggered at the first instant of contact between the pedestrian lower extremity and the vehicle. After positioning, the positions of the 6DOF cubes and of relevant anatomical landmarks were measured using a 3D coordinate measuring machine, as well as the position of the phototargets used for determining video imager resolution for the video analysis (see section Data processing – High speed video analysis). Immediately prior to the test, fingerpaint was applied to specific locations of the pedestrian so that the paint marks on the vehicle would depict specific contact points.

POST-TEST CT-SCAN AND AUTOPSY : After the test, a full body CT scan was performed (slice thickness: 0.625mm, in-slice resolution: 0.98 mm/pixel) to assess the lesions and to serve as a guide for the subsequent full-body necropsy.

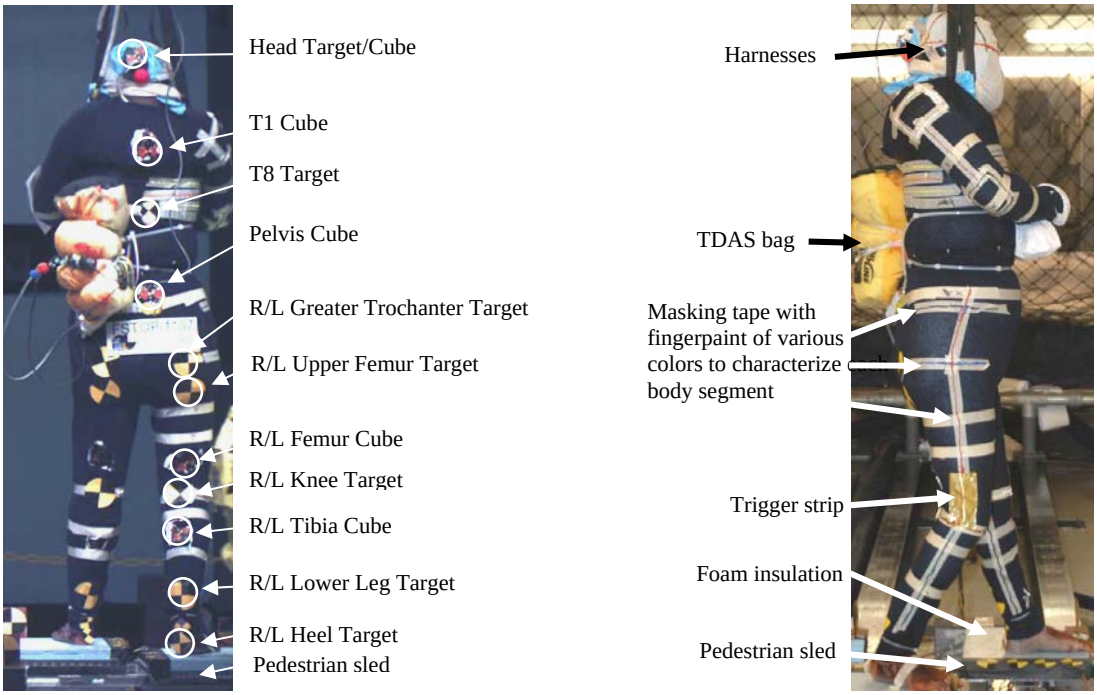


**Fig. 4 – *Left:* Phototarget locations, R/L: Right/Left. *Right*: Paint scheme on a subject ready for the test.**

## DATA PROCESSING

HIGH SPEED VIDEO ANALYSIS: Each phototarget (Fig. 4) was tracked from 20 ms prior to bumper contact to a few milliseconds beyond head contact using images from the posterior video camera that provided a view of the entire pedestrian. The spatial resolution of the imager was determined using pairs of phototargets fixed to the pedestrian sled prior to testing (Fig. 5). Pedestrian sled target distances were measured in millimeters using the CMM prior to testing and in pixels using the t=0 video image. To account for the variation in the spatial resolution as a function of the distance from the imager (i.e., parallax), pairs of targets at different distances from the imager were used to calculate the resolution as a function of the x-distance (Figure 5). Using the initial x location of each target affixed to the subject (from the pre-test CMM data), the spatial resolution of the image for each target was determined and multiplied by the position data (in pixels) to determine the trajectory of each target. The trajectories were assessed relative to the vehicle motion in order to calculate trajectories in the vehicle coordinate system (VCS).

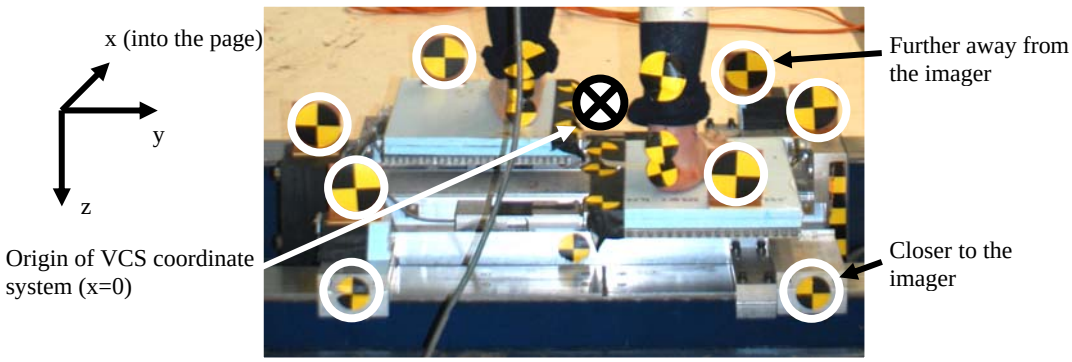


**Fig. 5 – Pedestrian sled with the phototargets for resolution calculation.**

INSTRUMENTATION DATA ANALYSIS : The CT images were used to determine the position and orientation of the L5 mount with respect to the L5 vertebral body for each subject, with the goal of expressing the angular velocities in a coordinate systems fixed with respect to L5. The objective was to eliminate the differences in the 6DOFP data that resulted from variations in mounting locations between specimens and to express the kinematics data in a standardized L5 coordinate system. The L5 coordinate system was defined using points on the following anatomical landmarks: the spinous process (P), and the

left and right transverse processes (L and R respectively) (Fig. 6). Since the position and orientation of the 6DOFP relative to the U mount was known, the position of the 6DOFP was determined in the L5 coordinate system. Finally, the angular rates were transformed to the L5 coordinate system.

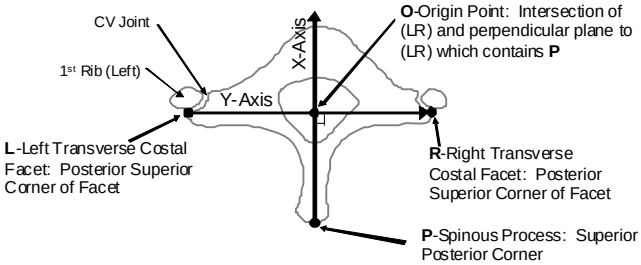


**Fig. 6 - Anatomical landmarks for the vertebra (T1 is shown). The z-axis is orthogonal to the x- and z-axis, point out of the page.**

## RESULTS

INITIAL POSITION **:** The position of the subjects immediately prior to the impact in the lateral and frontal planes was reproducible for all the tests with the exception of some of the lower limb joint angles (Figs. 7 and 8)

VEHICLE DEFORMATION : Using data collected with the CMM the vehicle deformation was calculated. The deformed and undeformed contours were plotted with longitudinal contours varying from -500 to 500 mm relative to the vehicle centerline with the x, y and z deformations (Appendix 1). In addition, the longitudinal contours with the greatest y and z deflections were superimposed to the undeformed contour of the vehicle.

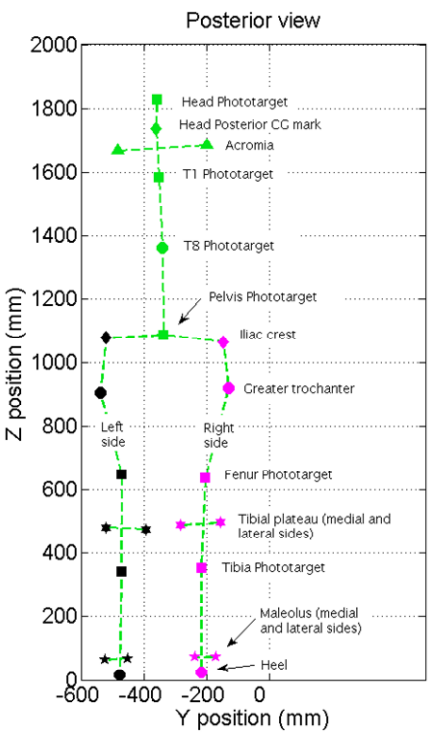


**Fig. 7 Anatomical Landmarks.**

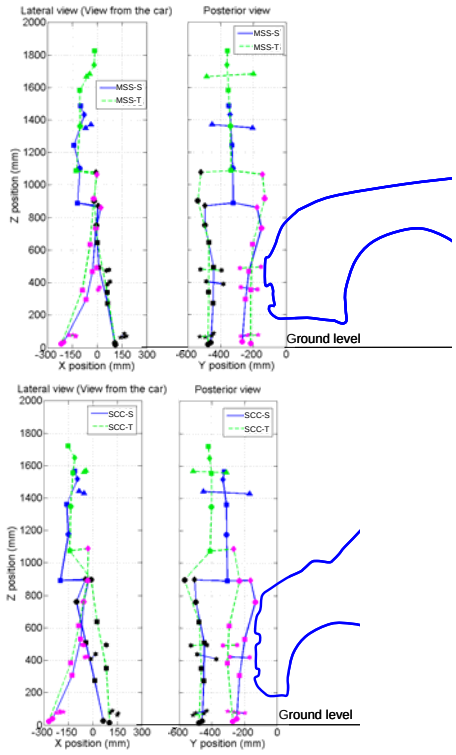


**Fig. 8. Initial positions, with the scaled front end of the vehicle for the mid sized sedan (top) and the small city car (bottom). The position of the left iliac crest could not be measured for SCC-T.**

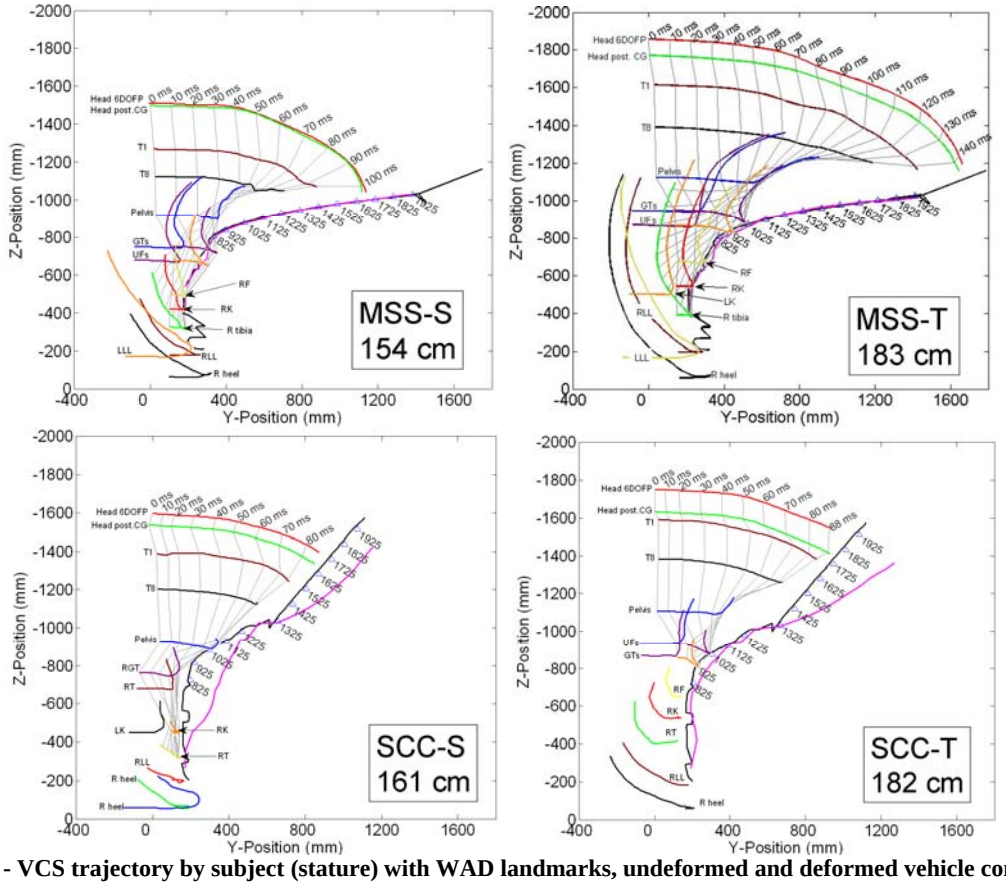


**Fig. 9 - VCS trajectory by subject (stature) with WAD landmarks, undeformed and deformed vehicle contours. GT: greater trochanter, UF: upper femur, F: femur, K: knee, T: tibia, LL: lower leg, R: right, L: left.**

VIDEO ANALYSIS AND HEAD INJURY CRITERION: The video data were analyzed in three coordinate systems. First, the trajectories of the phototargets were potted in the VCS to examine the pedestrian kinematics relative to the vehicle. Next, the photo trajectories were plotted relative to the pelvis phototarget trajectory to emphasize how the lower extremity and upper body trajectories were linked. Finally, a pelvis coordinate system was defined for every subject to describe the motion of each body segment relative to their adjacent body segments.

Trajectories in VCS: To facilitate analysis of the temporal aspects of the trajectories and the influence of the vehicle geometry on the impact kinematics (Fig. 9), adjacent body segment trajectories were connected at 10 ms intervals and plotted relative to the centerline contours of the vehicles (before and after deformation). The key difference between the trajectories of the short and the tall subjects can be reduced to how the pelvis motion affects both the upper body and the lower extremity kinematics. For the shorter subjects tested, a sharp change in the pelvis kinematics occurred when the pelvis contacted the hood occurred. The pelvis contact point was located on the front end of the vehicle (between the ground and the HLE), with the largest deformation produced in the Y direction. For the taller subjects, there was no drastic change in kinematics from pelvic contact with the vehicle because the pelvis went over the hood and produced the largest deformation in the Z direction.

The HIC, head maximum resultant accelerations (MRA) were determined and the head WAD were measured (Table 2) for each subject. Both HIC and MRA were higher for the short subjects with a given vehicle. An estimate of how much sliding occurred during the impact was calculated as the difference between the head WAD and the height of the subject. As expected from the vehicle deformation information, the extent of sliding was larger for the taller subjects.

Trajectories relative to the pelvis: The upper body kinematics relative to the lower extremity kinematics were further investigated by examining the trajectories of the head, T1, T8, right thigh, right femur, right knee, right tibia and right heel relative to the pelvis in the VCS coordinate system (Fig. 10). Any offset in the initial position of these phototargets corresponds to the position of the pelvis at time 0. Lines were used to connect adjacent body segments at 5 ms intervals with thicker lines added at the times of first vehicle contact between the right knee (RK), the right iliac crest (RIC), the elbow (El), the shoulder (Sh) and the head (Hd) (Table 3).

**Table 2 – Head impact data. Italic font is used for the shortest subjects for each vehicle.**

| | HIC | MRA* (g) | WAD* (mm) | Sliding estimate = WAD - height (mm) |
|---|---|---|---|---|
| *MSS-S* | *1730* | *167* | *1600* | *60* |
| MSS-T | 924 | 117 | 2125 | 295 |
| *SCC-S* | *716* | *163* | *1630* | *20* |
| SCC-T | 280 | 106 | 1900 | 80 |

*: MRA stands for maximum resultant acceleration, WAD for wrap around distance

At the time of head contact, the pedestrian angle of lateral bending (approximated as the acute angle formed in the y-z plane by the line connecting the pelvis to T1 and the line connecting the pelvis to the right heel) was larger for the short subjects (45˚ for MSS-S, 28˚ for SCC-S) than for the tall subjects (roughly 0˚ for both vehicles). The pedestrian angle is intended to provide a gross estimate of the extent to which the pedestrian is 'bent' at the time of head contact. For the shorter subjects, the lower extremity remained in contact with the vehicle until the RIC contacted the hood, whereas the lower limbs rebounded from the vehicle for the taller subjects. For the shorter subjects, wrapping of the lower extremity around the lower vehicle structures may have further inhibited the pelvis from sliding on the hood.

Trajectories in the pelvis coordinate system: The pelvis coordinate system was defined for each subject to assess the position of each body segment in a coordinate system attached to the body. Because there is little motion between L5 and the pelvis, the coordinate system with the L5 phototarget was chosen as the origin of the pelvis coordinate system. It was hypothesized the main rotation of the L5 vertebra occurred about the vertebra x-axis (Fig. 6), and that this axis was nearly aligned with the x-axis of the VCS. Thus, the degrees of freedom for the L5 vertebra in VCS were the translations in the y and z directions, as well as rotations about the x-axis. With these assumptions, the angular velocity about the L5 x-axis was integrated to obtain the orientation of the L5 vertebra in the y-z plan. Next, the orthogonal $X_{pelvis}$ and $Y_{pelvis}$ axes were calculated at each time step (Fig. 11).

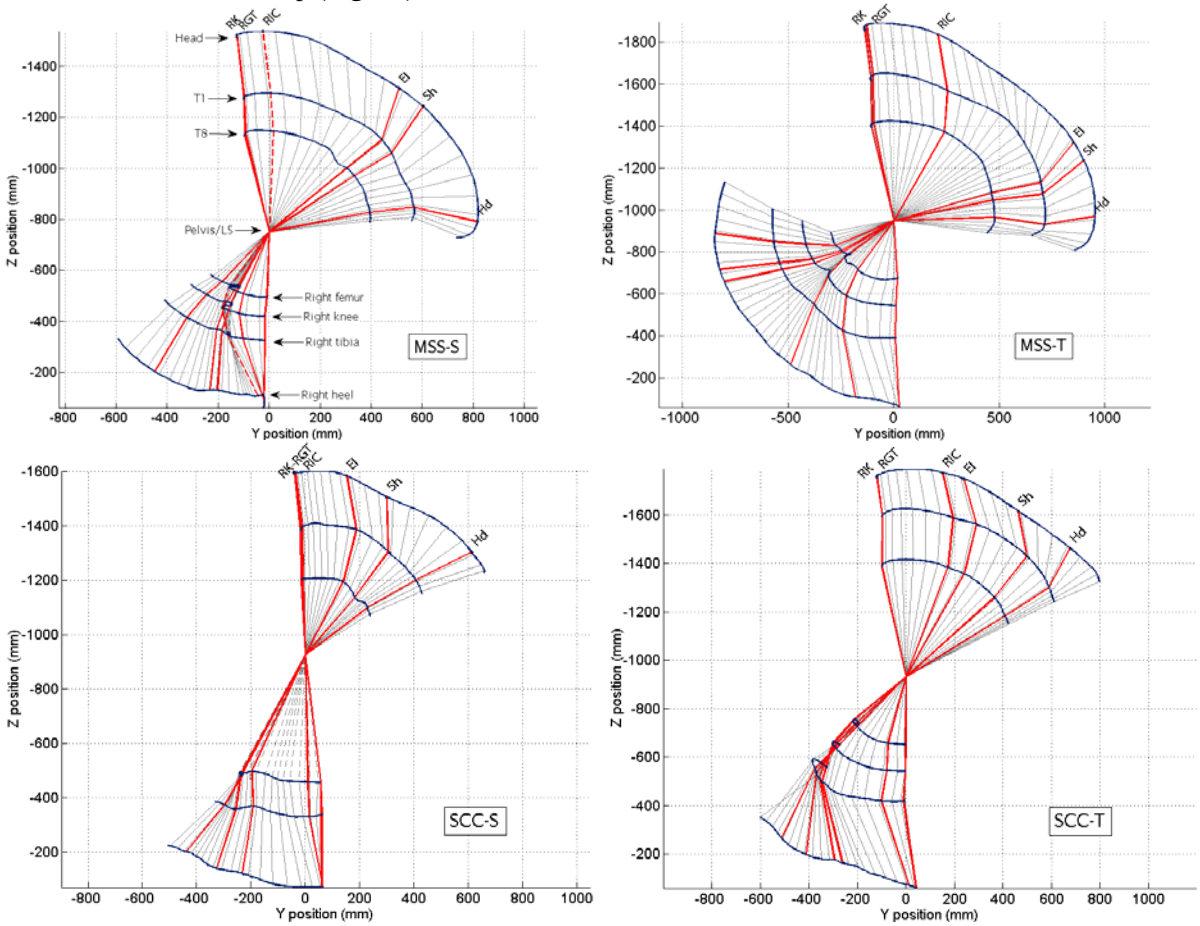


**Fig. 10 - Trajectories relative to the pelvis. The lines representing the contact times of the right knee (RK) and right greater trochanter (RGT) are close, and therefore the lines are superimposed.**

The trajectories were split into phases to highlight the changes in the trajectories that occurred. The trajectory of each body segment at 5 ms intervals was plotted in light grey while trajectories during the phase of interest were plotted in darker grey (examples shown Fig. 12) Arrows indicate the direction of motion for each body segment. Contact times of relevant body segments are provided in Table 3. The remaining plots for all test subjects and vehicles are provided in Appendix 2.

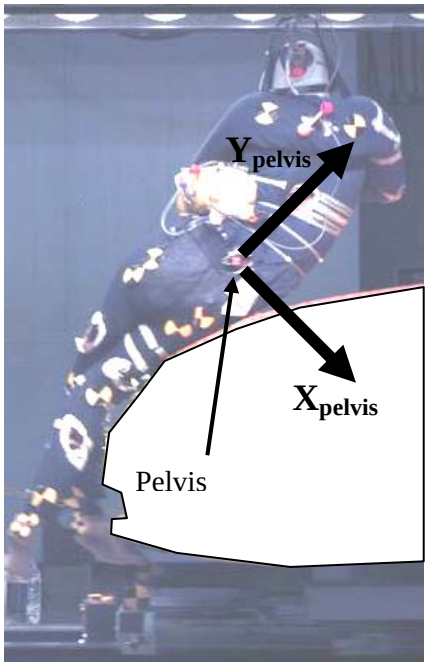


**Fig. 11 – Pelvis coordinate system.**

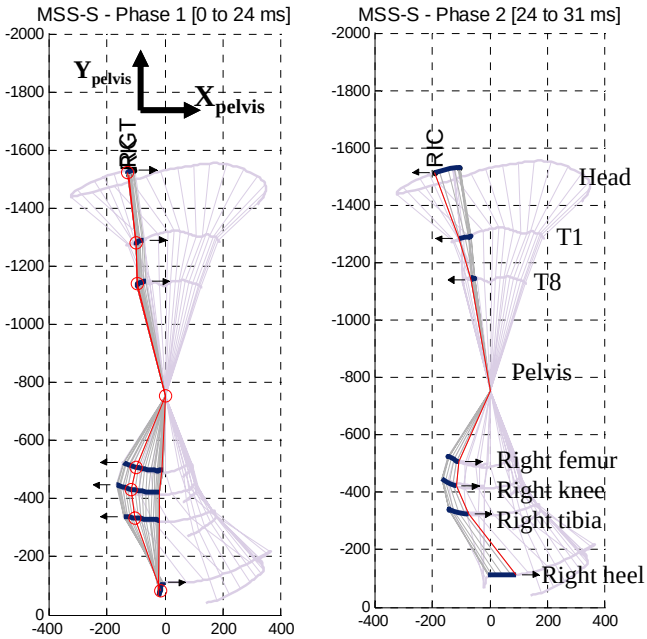


**Fig. 12- Trajectories in the pelvis coordinate system (MSS-S).**

For all the tests, the upper body moved very little until the RGT contacted the hood. After RGT contact, the spine bent in the direction of the vehicle motion until it reached a maximum bending angle. This maximum did not always relate to the contact of a more proximal body segment (Table 3) and it may represent a limit prescribed by the range of motion for the body segments involved.

**Table 3 - Time of first contact between the vehicle and the corresponding body segments.**

| | Right knee (RK) | Right greater trochanter (RGT) | Right iliac crest (RIC) | Elbow (El) | Shoulder (Sh) | Head (Hd) |
|---|---|---|---|---|---|---|
| MSS-S (ms) | 4 | 17 | 31 | 69 | 76 | 107 |
| MSS-T (ms) | 5 | 31 | 65 | 121 | 127 | 144 |
| SCC-S (ms) | 5 | 3 | 16 | 53 | 68 | 94 |
| SCC-T (ms) | 3 | 14 | 49 | 56 | 74 | 91 |

INJURY REPORT : The impacts generated injury in each subject with the distribution and extent of trauma dependent on the particular subject and vehicle tested. Pelvic and thoracic injuries are detailed in Appendix 3 while Fig. 13 provides an overall injury assessment for each subject. In assessing injury severity, it is important to recall that only the subject MSS-T had normal bone mineral density (BMD) (Table 1) while the other three subjects had poor bone mineral density. Despite the lower BMD, MSS-S sustained fractures of the pelvis and the thoracic vertebrae similar to those sustained MSS-T. When comparing across vehicle types, SCC-S and SCC-T subjects experienced more rib fractures than the MSS-T and MSS-S subjects.

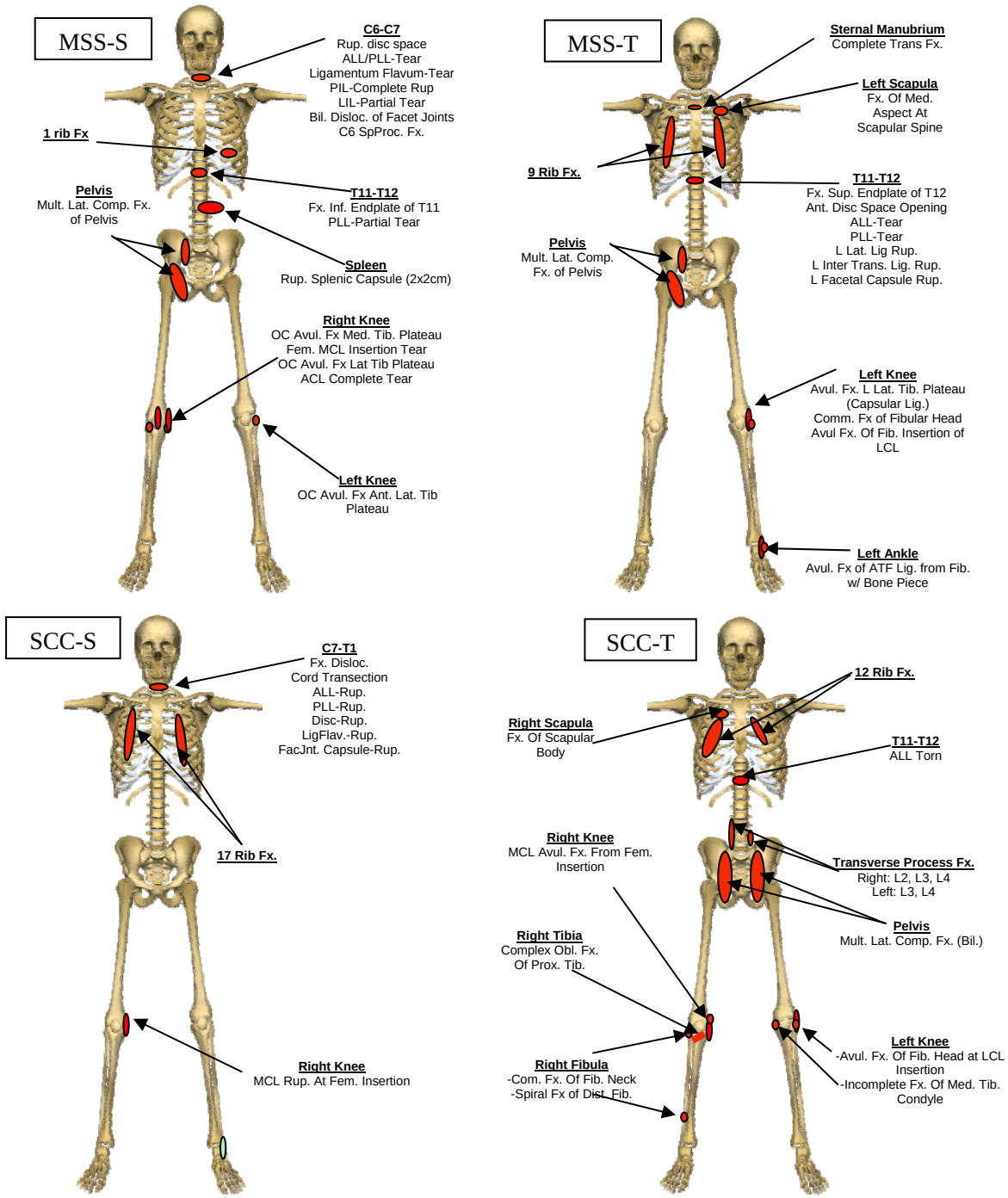


Ant — Anterior
ALL — Anterior Longitudinal Ligament
ATF—Anterior Talo-Fibular (Ligament)
Avul. — Avulsion
Bil.—Bilateral
CC — Costochondral as in Costrochondral Junction
Comp.— Compression
Com.— Comminuted
Disloc. — Dislocation
FacJnt. — Facet Joint
Fem. — Femur
Fib. — Fibula
Fx. — Fracture
Inf. — Inferior
L. — Left
Lat. — Lateral
Lig. — Ligament
LigFlav. — Ligamentum Flavum
LIL — Lateral Interspinous Ligaments
Med. — Medial
MCL — Medial Collateral Ligament
Mult. — Multiple
Obl. — Oblique
OC — Osteochondral
PIL — Posterior Interspinous Ligaments
PLL — Posterior Longitudinal Ligament
Pos. — Posterior
R. — Right
Rup. — Rupture
SpProc. — Spinous Process
SC — Sterno-Chondral
SI — Sacro-Illiac
Sup. — Superior
Tib. — Tibia
Trans. — Transverse

**Fig. 13- Subjects injury diagrams.**

## DISCUSSION

INJURY ANALYSIS :

Mid-sized sedan: While deformation of the vehicle was larger at the pelvis contact area in the y and z directions for MSS-T than for MSS-S (Appendix 1, Fig. 18), the pelvis/vehicle contact occurred in two locations for MSS-S whereas it occurred in only one location for MSS-T. For MSS-S, the RGT contacted the hood right below the hood leading edge (HLE), whereas the RIC impacted the hood above the HLE based on the marks left on the hood by the fingerpaint. The two impacts resulted in large deformations in the y-direction below the HLE (RGT impact location) and in the z-direction above the HLE (RIC impact location; Appendix 1, Fig. 18). Both MSS-S and MSS-T subjects sustained injuries to the right pubic ramus, which likely resulted from direct impact with the hood. For MSS-S, the pubic ramus fracture may have been caused by the beam supporting the hood latch below the HLE level (deformation in the y-direction). Contact of the pubic ramus with the beam would have resulted in the RIC impacting the lower part of the hood above the HLE level. For MSS-T, the largest deformations occurred at the location where the RGT contacted the hood and resulted in the hood being pushed vertically downward and toward the windshield (Fig. 14).

As previously indicated, the kinematics of the pelvis dictated, to a large extent, the kinematics of the upper body. The video analysis showed that the elastic deformation of the hood was greater for MSS-T than for MSS-S (Fig. 15). Because of the impact of the pelvis, the hood deformed and stored elastic energy which was subsequently released when the load to the pelvis contact point decreased. This resulted in the pelvis rebounding from the hood and eventually losing contact. Subsequently, the thorax and the shoulder aligned in a 'flat' configuration (the thorax-shoulder line was roughly parallel to the hood centerline) and struck the hood simultaneously (Fig. 16) causing considerable deformation to the hood. In addition to the vehicle deformation, this impact was considered the source of the numerous bilateral rib fractures (Fig. 13). A few milliseconds following the torso contact with the hood, the head impacted the windshield. As in the case of the MSS-S, the pelvis stayed in contact with the hood and the shoulder impacted the hood before the thorax (Fig. 16), thereby potentially protecting the rib cage (only one rib fracture was reported).

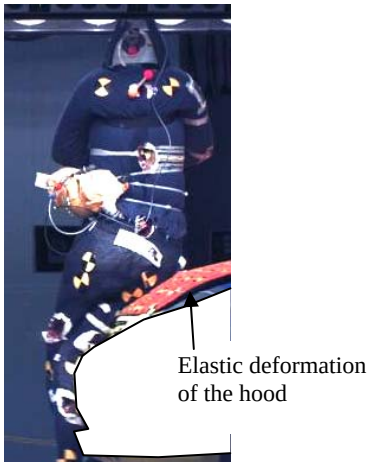


**Fig. 14- Elastic deformation of the hood because of the RGT impact (MSS-T).**

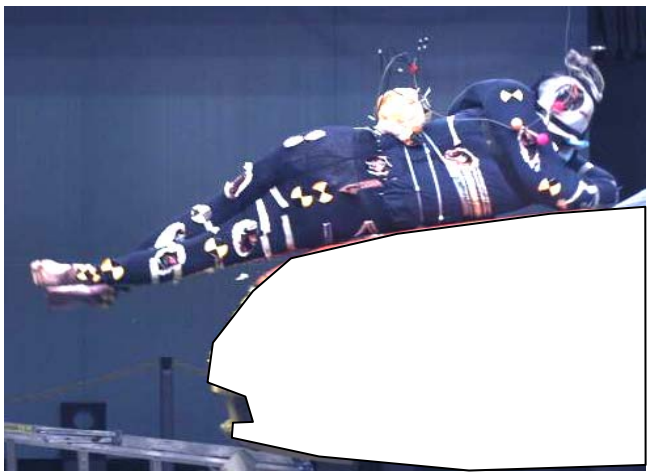

**Fig. 15- Thorax and shoulder simultaneous impact (MSS-T).**

Injuries at the T11-T12 junction were reported for both MSS tests. While latero-medial bending of the spine was generally large (Appendix 2), the extent of lateral bending was shown to depend on the pelvic interaction with the vehicle. When the pelvis or the RGT impacted the hood, the pelvis rotated about the antero-posterior axis of the subject which, in turn, triggered upper body rotation. During this motion, the head remained inertially fixed in space while the spine was bent towards the left aspect of the subject's body (phase 4 for MSS-S, phase 3 for MSS-T, appendix 2), potentially causing the thoracic spine injuries.

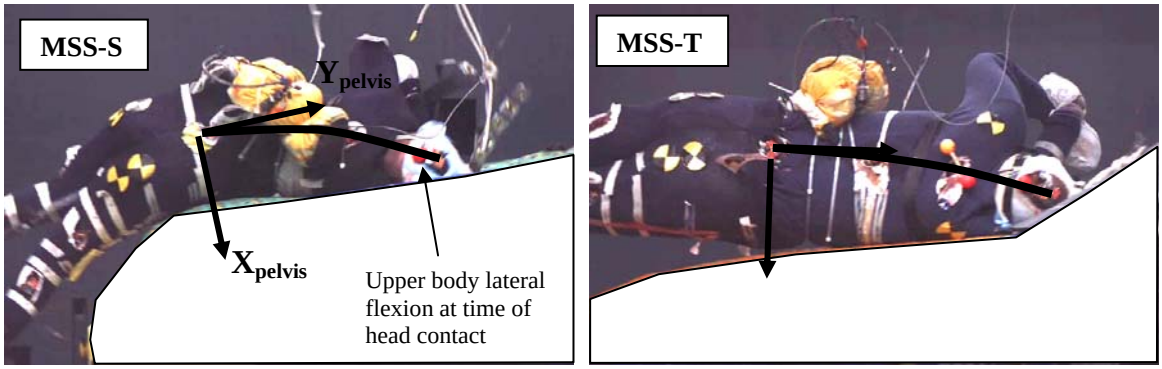


**Fig. 16 - Position of the head at time of head contact. The line connects the pelvis, T8, T1 and the head phototargets. The the pelvis coordinate system is plotted to be used for reference to evaluate the lateral flexion of the spine.**

As for the cervical injury for MSS-S, it was likely caused by the head hitting the hood and not the windshield (contrary to MSS-T, Fig. 16). In the case of MSS-S, the head continued to move towards the hood following initial shoulder contact, thereby producing lateral bending of the neck. Bending of the neck did not occur with MSS-T because the head impacted the windshield rather than the hood. The relative geometry of the shoulder and hood impact relative to that of the head and windshield impact prevented large angles of lateral bending of the neck and may have prevented neck injuries.

Small city car: Large deformations of the vehicle were observed in tests with both subjects. It is hypothesized that impacts with the SCC were less injurious for the pedestrian than those with the MSS because more deformation occurred in the front-end structure of the vehicle. As a result, only one right knee fracture was reported for SCC-S lower extremity. The contact area of the lower extremity with the front end of the vehicle was more localized for SCC-T than for SCC-S (Appendix 1). Because of the osteoperotic bone structures for SCC-T, the lower extremity was likely unable to resist the load applied by the front end of the vehicle, resulting in numerous injuries.

Multiple rib fractures were reported for both tests with the SCC. For SCC-S, the top edge of the hood contacted the torso below the rib cage (Fig. 17) while the rib cage impacted the windshield. At the time of rib cage contact, the thorax was roughly parallel to the windshield and resulted in planar (i.e., wall-type) loading to the chest. The same type of loading occurred for SSC-T, with the thoracic contact at an even higher level on the windshield.

For the two SSC tests, the mechanism for the vertebral injuries to the thorax is unclear. Based on the video analysis, the transverse process injuries to the lumbar spine may have occurred when the pedestrian's body was bending toward the right side. This motion would put the left side in tension, and the connected ligament could avulse from the transverse processes.

UPPER BODY KINEMATICS : Following application of load from vehicle to the pelvis, the forces were transmitted to the more proximal body structures. Because of the inertia of each body segment and the compliance of the connections between adjacent body segments, motion of the head, T1 and T8, was generally delayed from the pelvic motion (Appendix 2). This behavior, however, was highly dependent on subsequent interaction of these body regions with the vehicle components. At the time of head impact, the head motion lead that of T1 and T8 for the shortest subjects, whereas it was behind T1 for the tallest subjects. This difference in head motion relative to the upper thoracic spine resulted from the differences in the position of the head relative to T1 before the time of contact that were produced by the local geometry of the vehicle in the vicinity of shoulder and head contact. At that time the head struck the vehicle, the necks of the shorter subjects were bent towards the vehicle whereas the necks of the taller subjects were bent away from the vehicle (Fig. 17).

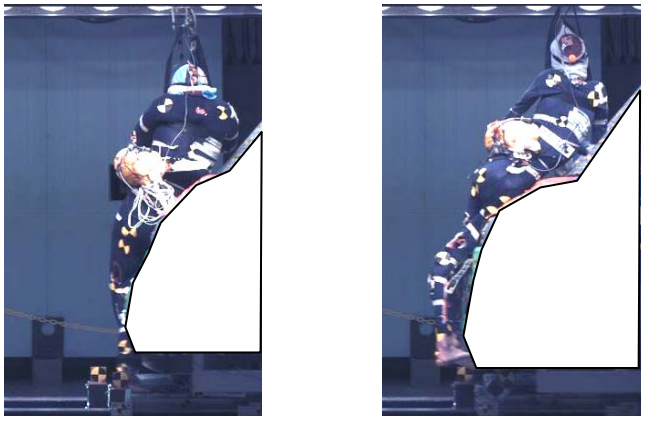

**Fig. 17- Thorax impact for SCC-S (*left*) and SCC-T (*right*).**

LIMITATIONS OF THE STUDY

Kinematic analysis : The kinematic analysis was performed using video data which are the projection of the scene onto the plane that the camera recorded (the subject frontal plane at time 0). Therefore, rotation about the longitudinal axis of the subjects, rotation about the latero-medial axis, or displacement in the antero-posterior (x-axis) direction would alter the trajectories measures. While variation of the camera resolution as a function of the x-distance (Fig. 5), specific resolutions was determined for each phototarget depending on their initial position measured with the CMM, the resolution for a given phototarget was not corrected for out-of-plane motion that occurred during the impact event.

Pelvis orientation : The x-axis defined from the L5 vertebral landmarks (Fig. 6) was assumed to be aligned with the x-axis in VCS. While the largest motion clearly occurred in the frontal plane, kinematics of the subject out-of-plane would change the definition of the L5 coordinate system.

Injury reports: Injuries to the thoracic and abdominal viscera were not observed. Given the extent of musculoskeletal injuries, the lack of visceral injury may have been influenced by the difficulty of identifying these injuries in cadaveric subjects. In terms of the extent of bony fractures observed, the subjects in the study were of advanced age and, moreover, all but one subject (MSS-T) had diminished bone quality. Despite these bone quality differences, however, injury patterns and severity were similar among subjects tested with a given vehicle..

Vehicle deformation: The deformation maps provided in Appendix 1 provide estimates of only the plastic deformation measured post-test. The elastic deformation was not measured directly and can only be estimated qualitatively from the video data. As previously noted, however, the elastic return of energy from the deformed hood components did result in changes to the upper body kinematics (MSS-T). The absence of engine did not affect the kinematics measured during the MSS-tests because the stiff front end structure prevented large deformations from occurring (i.e., given the measured post-test deformations the hood would have not contacted the engine if it had been present). The SCC tests caused much larger hood deformation, however, and it is likely that the deforming hood would have contacted the engine if it had been present. In addition to preventing higher loads from being applied to the pelvis, the absence of engine likely allowed greater deformation of the hood which, in turn, resulted in the less pedestrian lateral flexion of the upper body and sliding of the pelvis on the hood.

## CONCLUSION

The pedestrian-vehicle impact was analyzed using four cadaver tests performed with two vehicles. The trajectories for each subject were expressed in the vehicle and pelvis coordinate systems to examine the pedestrian impact as a function of the vehicle motion and the kinematics of adjacent body structures. The coordinate system attached to the pelvis was found to be useful in understanding the kinematics of the body segments relative to each other and in determining how and when injuries occurred. Using video and 6DOFP data, the kinematics of the pelvis as a function of the subject stature relative to the vehicle geometry were determinants of the overall upper body kinematics (head, T1 and T8 trajectories). Most documented injuries could be explained by interpreting the body region kinematics and the associated contact with vehicle structures. Despite variations in anthropometry and bone quality among subjects, consistent injury mechanisms were identified.

**ACKNOWLEDGEMENT**

The authors would like to thank the students involved in these tests (Chris Drinkwater, Check Kam, Robert Kendall, Benjamin Renzo) for their dedication and late hours work; Bernard Haxel, Mark McCardell and Jim Bolton for their reactivity to solve technical issues; Jay Evans for his contribution to the subjects preparation and necropsy, and Hervé Guillemot for the coffee talks about this study.

**REFERENCES**

Anderson RWG, Streeter LD, Ponte G., McLean AJ (2007). Pedestrian reconstruction using multibody madymo simulation and the Polar-II dummy: comparison of head kinematics, ESV conference, Lyon, France, 2007.

Bunketorp O, Romans B, Hansson T, Aldman B, Thorngren L, Eppinger R. (1983). Experimental study of a compliant bumper system. Proc. 27th STAPP Car Crash Conference. Society of Automotive Engineers, Warrendale PA. SAE-831623 Oct 1983, p. 287-297

European Enhanced Vehicle-Safety Committee (1998) EEVC Working Group 17 Report—Improved Test Methods to Evaluate Pedestrian Protection Afforded by Passenger Cars. www.eevc.org, December 1998.

Kam C, Kerrigan J, Meissner M, Drinkwater C, Murphy D, Bolton J, Arregui C, Kendall R, Ivarsson J, Crandall J, Deng B, Wang JT, Kerkeling C, Hahn W (2005). Design of a full-scale impact system for analysis of vehicle pedestrian collisions. Paper 2005-01-1875, Society of Automotive Engineers, Warrendale, PA.

Kallieris D, Schmidt G (1988). New aspects of pedestrian protection loading and injury pattern in simulated pedestrian accidents. Proc. of 32nd Stapp Car Crash Conference. Society of Automotive Engineers, Warrendale, PA. SAE-881725, p. 185-196.

Kerrigan J, Kam C, Drinkwater C, Murphy D, Bose D, Ivarsson J, Crandall J (2005a). Kinematic Comparison of the Polar-II and PMHS in Pedestrian Impact Tests with a Sport-Utility Vehicle. Proc. International Conference on the Biomechanics of Impacts (IRCOBI).

Kerrigan J, Murphy DB, Drinkwater DC, Kam CY, Bose D, Crandall J (2005b). Kinematic corridors for PMHS tested in full-scale pedestrian impact tests. NHTSA, Paper 05-0394, Proc. 19th Conference on the Enhanced Safety of Vehicles (ESV), Washington DC, United States.

Kerrigan J, Crandall J, Deng B (2007). Pedestrian kinematic response to mid-sized vehicle impact. International Journal of Vehicle Safety, 2(3): 221 – 240.

Kerrigan J, Rudd R, Subit D, Untaroiu C, Crandall J (2008). Pedestrian lower extremity response and injury: a small sedan vs. a large SUV. SAE Paper 2008-01-1245.

Masson C, Serre T, Cesari D (2007). Pedestrian-vehicle accident: analysis of 4 full-scale tests with PMHS. ESV conference, Lyon, France, 2007.

Meissner M, van Rooij L, Bhalla K, Crandall J, Longhitano D, Takahashi Y, Dokko Y, Kikuchi Y (2004). A Multi-Body Computational Study of the Kinematic and Injury Response of a Pedestrian with Variable Stance upon Impact with a Vehicle, SAE Paper 2004-01-1607.

Robbins DH (1983). Anthropometric Specifications for Mid-Sized Male Dummy, Volume 2. University of Michigan Transportation Research Institute (UMTRI) report number UMTRI-83-53-2.

Rudd R, Kerrigan J, Crandall F, Arregui C (2006). Kinematics analysis of head/neck motion in pedestrian-vehicle collisions using 6-degree-of-freesom instrumentation cubes, SAE Paper 2006-01-0681

SAE J211/1 (1995). Instrumentation for Impact Test—Part 1—Electronic Instrumentation, SAE.

Serre T, Masson C, Perrin C, Chalandon S, Llari M, Cavallero C, Py M, Cesari D (2006), Pedestrian and cyclist accidents: a comparative study using in-depth investigation, multibody simulation and experimental test, Proc. International Conference on the Biomechanics of Impacts (IRCOBI).

Untaroiu C, Kerrigan J, Kam C, Crandall J, Yamazaki K, Fukuyama K, Kamiji K, Yasuki T, Funk J. (2007), Correlation of strain and loads measured in the long bones with observed kinematics of the lower limb during vehicle-pedestrian impacts. Stapp Car Crash Journal. Vol. 51.

World Bank (2003). Road safety at a glance. http://web.worldbank.org/WBSITE/EXTERNAL/TOPICS/EXTHEALTHNUTRITIONANDPOPULATION/EXTPHAAG/0,,contentMDK:20780317~menuPK:64229809~pagePK:64229817~piPK:64229743~theSitePK:672263,00.html#PDF

## APPENDICES

A color version of the appendices can be downloaded from http://www.centerforappliedbiomechanics.org/publications.html/subit08_ircobi_appendices.pdf

APPENDIX 1: 3D PLOT OF THE VEHICLE DEFORMATION

The following figures show a map of the vehicle deformation. In the y and z directions, a positive deformation depicts that the corresponding point moved into the car. In the x direction, the deformations are defined as (position in the deformed configuration – position in the undeformed configuration). The scale of the colormap is different for each plot because of the large variation in the ranges of deformation. The deformations are expressed in millimeters.

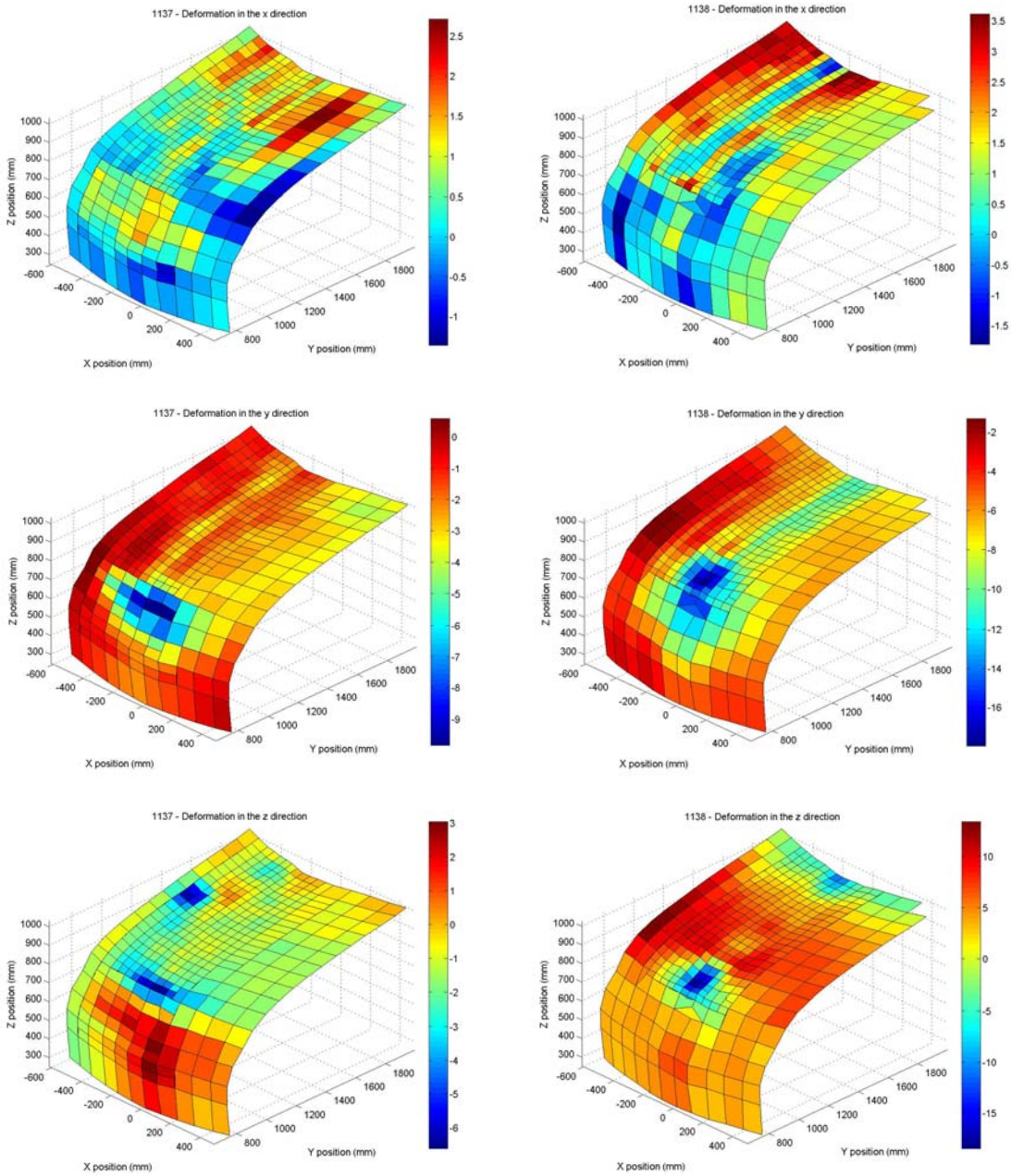


**Fig. 18 - Deformed front end of the MSS. *Left*: MSS-S, *right*: MSS-T**

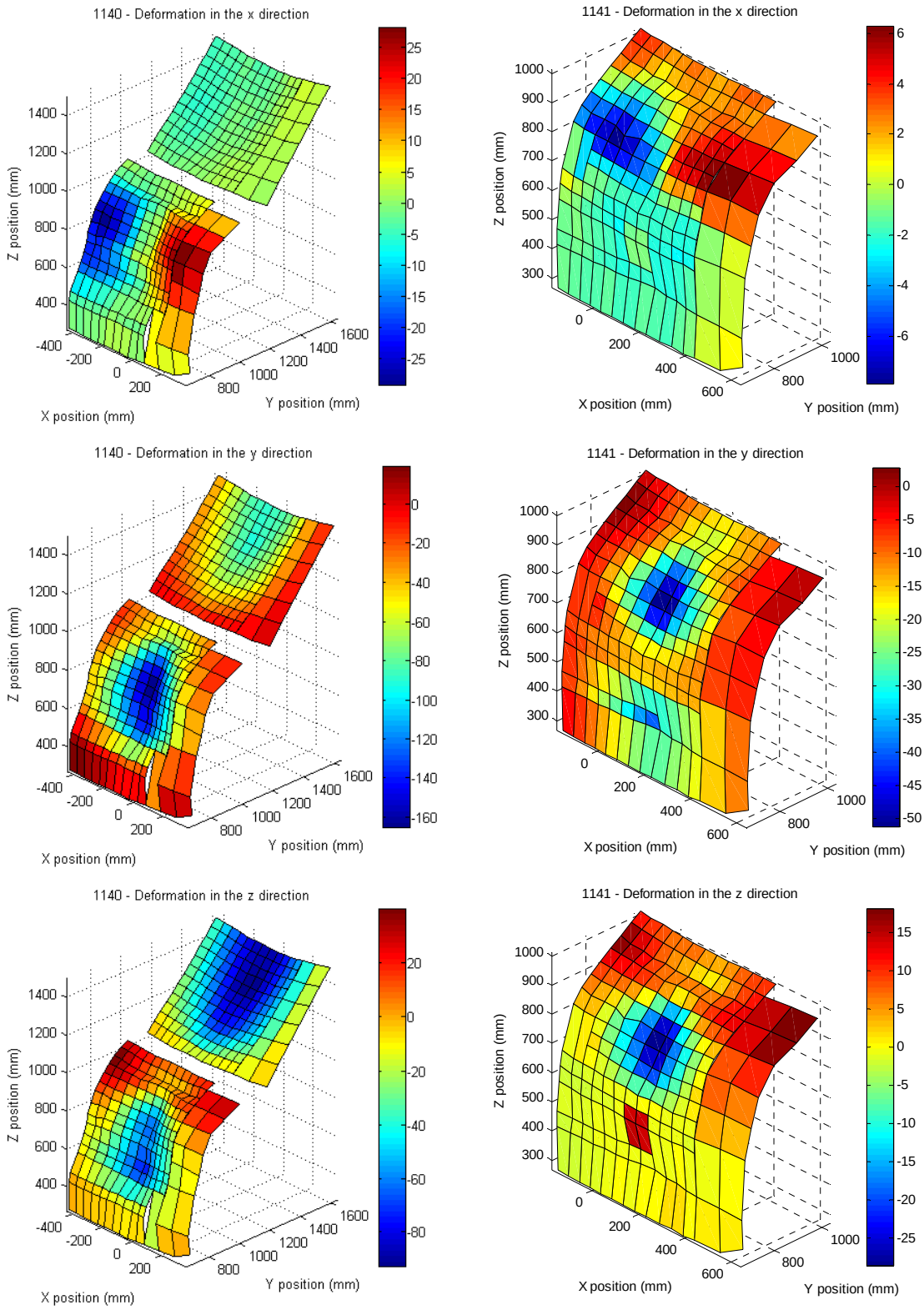


**Fig. 19- Deformed front end of the SCC. *Left*: SCC-S, *right*: SCC-T. For SCC-T, only the data below the hood top edge were exploitable.**

APPENDIX 2: TRAJECTORIES IN PELVIS COORDINATE SYSTEM

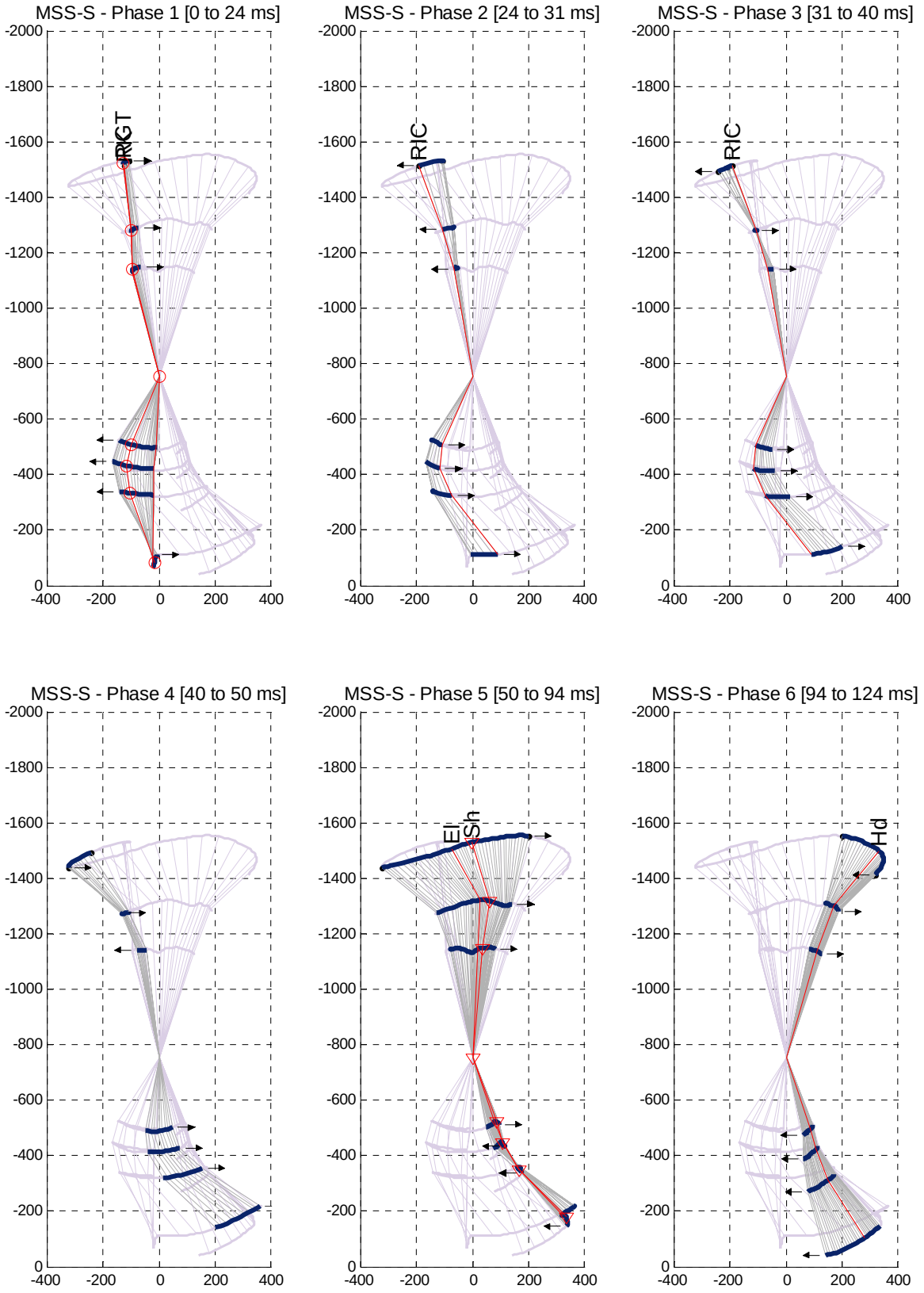


**Fig. 20 - Trajectories in the pelvis coordinate system (MSS-S)**

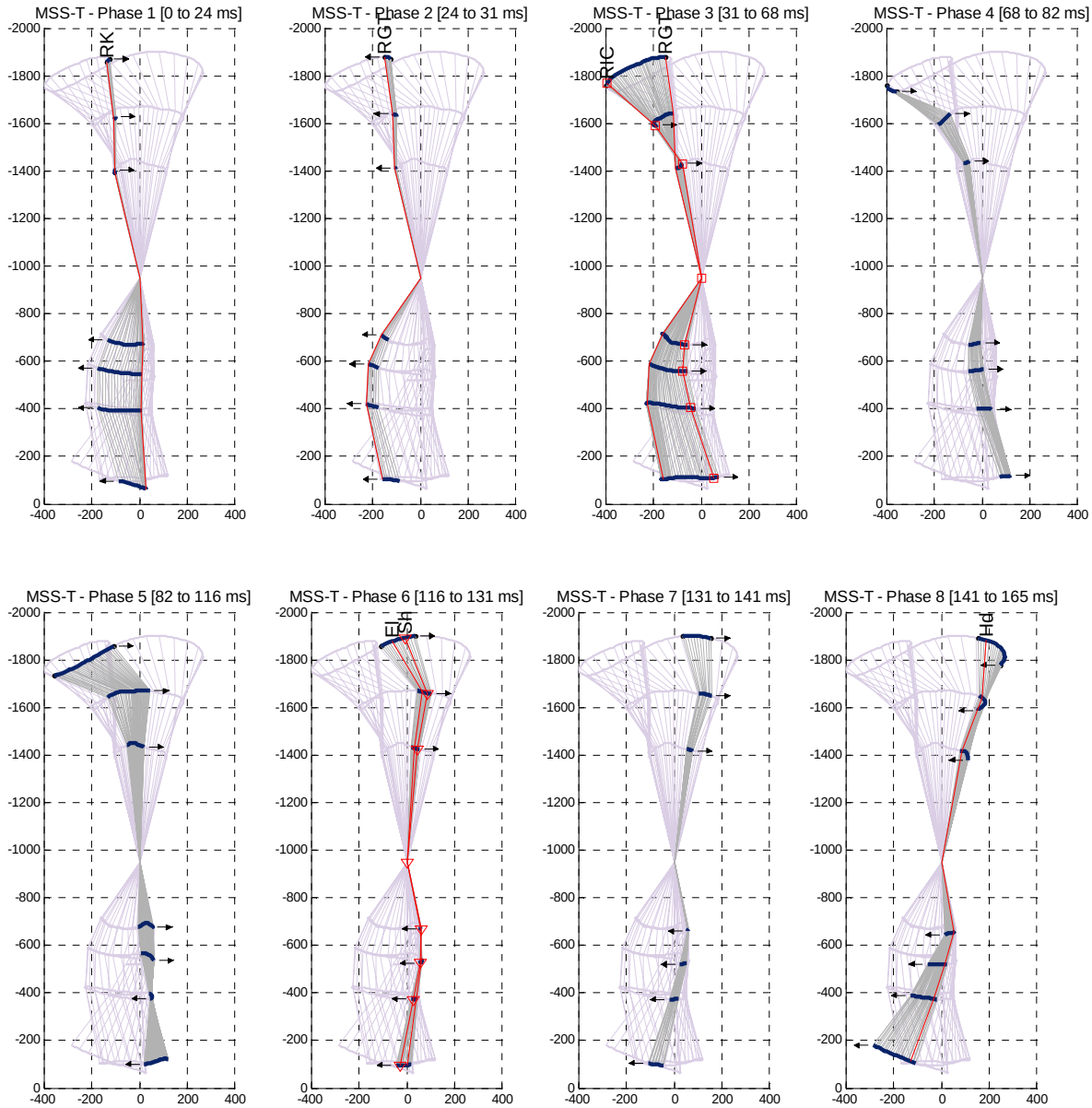


**Fig. 21 - Trajectories in the pelvis coordinate system (MSS-T)**

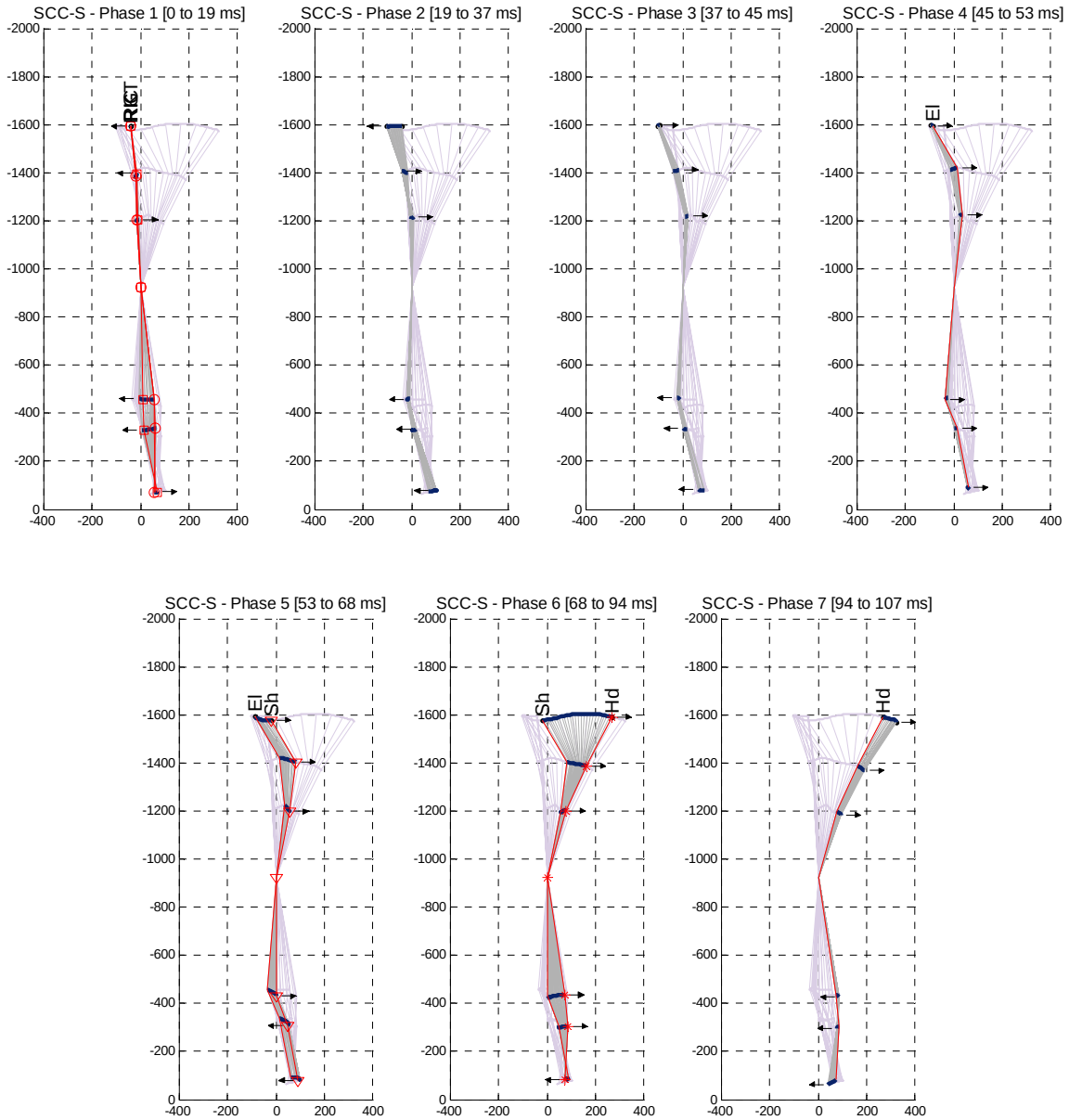


**Fig. 22 - Trajectories in the pelvis coordinate system (SCC-S).**
**No data could be collected for the right femur.**

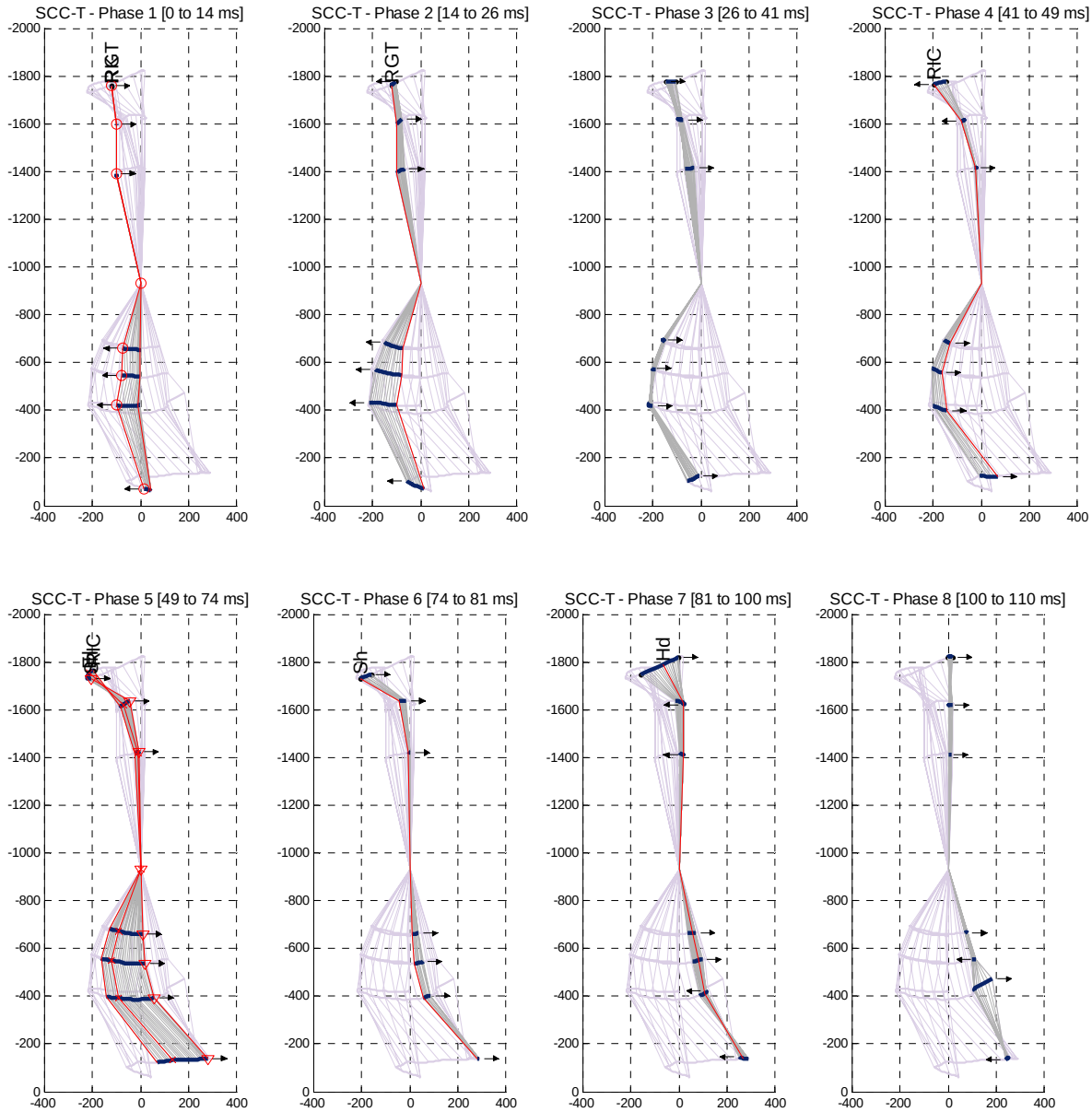


**Fig. 23 - Trajectories in the pelvis coordinate system (SCC-T)**

APPENDIX 3: DETAILED REPORTS OF PELVIS AND THORAX INJURIES

The same abbreviations as the ones defined in Fig. 13 are used here. The top left pictures are the right and left views of the pelvis, the bottom left pictures are the posterior and anterior views of the pelvis, and the right pictures are the anterior and posterior views of the thorax.